Applied Physics Letters

Photoluminescence from $InSb_{1-x}Bi_x$ alloys at extended wavelengths on InSb

Cite as: Appl. Phys. Lett. **121**, 191901 (2022); https://doi.org/10.1063/5.0121657
Submitted: 18 August 2022 • Accepted: 13 October 2022 • Published Online: 08 November 2022

R. C. White, L. J. Nordin, A. J. Muhowski, et al.

AIP Publishing

Applied Physics Letters ARTICLE scitation.org/journal/apl

Photoluminescence from $InSb_{1-x}Bi_x$ alloys at extended wavelengths on InSb

Cite as: Appl. Phys. Lett. **121**, 191901 (2022); doi: 10.1063/5.0121657
Submitted: 18 August 2022 · Accepted: 13 October 2022 ·
Published Online: 8 November 2022

R. C. White,[1,a)] L. J. Nordin,[2] A. J. Muhowski,[1] D. Wasserman,[1] and S. R. Bank[1]

AFFILIATIONS

[1]Microelectronics Research Center and the Electrical and Computer Engineering Department, The University of Texas at Austin, Austin, Texas 78758, USA
[2]Geballe Laboratory for Advanced Materials, Stanford University, Palo Alto, California 94305, USA

[a)]Author to whom correspondence should be addressed: coreywhite@utexas.edu

ABSTRACT

The incorporation of dilute concentrations of bismuth into traditional III–V alloys produces significant reductions in bandgap energy presenting unique opportunities in strain and bandgap engineering. However, the disparity between the ideal growth conditions for the host matrix and those required for substitutional bismuth incorporation has caused the material quality of these III–V–Bi alloys to lag behind that of conventional III–V semiconductors. $InSb_{1-x}Bi_x$, while experimentally underexplored, is a promising candidate for high-quality III–V–Bi alloys due to the relatively similar ideal growth temperatures for InSb and III–Bi materials. By identifying a highly kinetically limited growth regime, we demonstrate the growth of high-quality $InSb_{1-x}Bi_x$ by molecular beam epitaxy. X-ray diffraction and Rutherford backscattering spectrometry (RBS) measurements of the alloy's bismuth concentration, coupled with smooth surface morphologies as measured by atomic force microscopy, suggest unity-sticking bismuth incorporation for a range of bismuth concentrations from 0.8% to 1.5% as measured by RBS. In addition, the first photoluminescence was observed from $InSb_{1-x}Bi_x$ and demonstrated wavelength extension up to 7.6 μm at 230 K, with a bismuth-induced bandgap reduction of ∼29 meV/% Bi. Furthermore, we report the temperature dependence of the bandgap of $InSb_{1-x}Bi_x$ and observed behavior consistent with that of a traditional III–V alloy. The results presented highlight the potential of $InSb_{1-x}Bi_x$ as an alternative emerging candidate for accessing the longwave-infrared.

Over the past few decades, III–V–bismide alloys have received much attention due to the significant bandgap reduction induced by the incorporation of small concentrations of bismuth.[1,2] These dilute-bismide alloys have facilitated wavelength extension for a variety of applications including solar cells,[3] lasers,[4] and photodetectors.[5] However, dilute-bismides continue to be plagued by poor material quality relative to traditional III–V alloys, often attributed to the dissimilar growth temperatures of the optimized host matrix and its dilute-bismide counterpart. To overcome the disparity in growth window, both low substrate temperatures and V/III flux ratios near stoichiometry are necessary to promote bismuth incorporation due to the generally weak strength of III–Bi bonds as opposed to other III–V and Bi–Bi bonds.[6–8]

InSb, thus, may present a unique opportunity for dilute-bismides, as the In–Sb bond strength is the lowest of the conventional III–V materials.[8] As a result, the optimal growth temperature for InSb is likewise low,[9] and, therefore, the deviation in growth conditions for $InSb_{1-x}Bi_x$ from those of InSb should be comparatively small. Additionally, Sb and Bi possess remarkably similar electronegativities resulting in minimal differences in covalent bonding between InSb and InBi.[10] Furthermore, there is a relatively small mismatch in lattice constant between InBi[11,12] and InSb, particularly when compared with other dilute-bismide host matrices. The small lattice mismatch between InBi and InSb, in conjunction with the similarities in bond strength and electronegativities, could lead $InSb_{1-x}Bi_x$ alloys to potentially exhibit behavior that is more consistent with conventional III–V semiconductor alloys, rather than highly mismatched alloys. If $InSb_{1-x}Bi_x$ were not a true highly mismatched alloy, it would not necessarily exhibit band anticrossing or a "penalty" in optical quality with increasing bismuth incorporation. Thus, high-quality $InSb_{1-x}Bi_x$ could potentially be realized without the extreme reduction in material quality typically observed in other highly mismatched materials. However, more experimental work is necessary to determine whether $InSb_{1-x}Bi_x$ demonstrates conventional or highly mismatched alloy characteristics.

In addition to the potential compatibility of bismuth incorporation in InSb, $InSb_{1-x}Bi_x$ is a particularly promising candidate for

accessing the long-wave infrared (LWIR, 8–14 μm) with high-performance optoelectronic devices. While considerable wavelength extension beyond that of the host matrix has been shown in many other dilute-bismide alloys,[13–17] there are no reports of emission at, or beyond, that of native InSb from any other dilute-bismide alloys. InSb inherently possesses the narrowest bandgap energy of any conventional III–V alloys and, thus, $InSb_{1-x}Bi_x$ is expected to span the entire LWIR with only ~5% Bi incorporation.[12] All in all, $InSb_{1-x}Bi_x$ presents an opportunity for a direct transition, lattice-matched, LWIR III–V material, which is a spectral regime currently dominated by either other material systems, such as HgCdTe, or more complicated and weaker absorbing III–V materials employed in type-II superlattices and quantum well infrared photodetectors.[18,19]

Despite promising material and optical advantages, $InSb_{1-x}Bi_x$ remains underexplored relative to wider bandgap dilute-bismides with comparatively few experimental studies since the alloy was first synthesized over 50 years ago.[11] In the investigations that have been performed, there are conflicting reports on basic material properties. The lattice has been reported to both contract[20,21] as well as expand[11,12,22] with bismuth incorporation and reports of the bismuth-induced bandgap reduction range from 6[23] to 35 meV/% Bi[12] based on room-temperature optical absorption measurements. Moreover, there are no systematic studies of the full growth space for $InSb_{1-x}Bi_x$ and many important properties and parameters that are necessary for the device design have yet to be experimentally demonstrated. In particular, epitaxial growth in the "unity-sticking" regime[24] has yet to be demonstrated, despite growth under such a regime being a prerequisite for yielding high optical quality from highly mismatched alloys, such as dilute-bismides, dilute-borides, and dilute-nitrides. In this work, we report the growth of high-quality $InSb_{1-x}Bi_x$ films that exhibit unity-sticking bismuth incorporation, which enabled the observation of photoluminescence (PL) from $InSb_{1-x}Bi_x$ alloys.

Nominally 250 nm thick epitaxial films were grown on n-type InSb (100) substrates by solid-source molecular beam epitaxy (MBE). The films were grown in a Varian Gen-II MBE system, which is equipped with a valved cracker cell for antimony and dual-zone thermal effusion cells for indium and bismuth. Prior to growth, substrates were thermally deoxidized at ~425 °C under an antimony overpressure. To promote bismuth incorporation, low substrate temperatures and V/III flux ratios near stoichiometry were maintained during the growth of the $InSb_{1-x}Bi_x$ films to reduce bismuth desorption and minimize Sb/Bi competition.[6,11] Building on the work of Ptak *et al.* on $GaAs_{1-x}Bi_x$,[25] a relatively fast growth rate was employed to mitigate bismuth droplet formation by kinetically limiting excess bismuth accumulation on the surface during growth. Under the same growth conditions, ten $InSb_{1-x}Bi_x$ films were grown with varying Bi/III flux ratios by changing only the bismuth beam equivalent pressure (BEP) between 5×10^{-9} and 2.7×10^{-8} Torr. During the growth of the $InSb_{1-x}Bi_x$ films, the substrate temperature was approximately 300 °C as measured by blackbody thermometry with a kSA BandiT system. The indium flux corresponded to a growth rate of ~1 μm/hr at a BEP of 5.06×10^{-7} Torr. The antimony BEP was 9.04×10^{-7} Torr for an Sb/In flux ratio of 0.975×, based on V-limited reflection high-energy electron diffraction (RHEED) oscillations of GaSb at a similar substrate temperature to that employed during InSb(Bi) growth.

Atomic force microscopy (AFM) was used to quantify the roughness of sample surfaces and determine if bismuth droplets had formed. Figure 1 shows the RMS roughness of each film with inset AFM surface morphology measurements shown for the samples grown with the highest two bismuth BEPs. There is a clear minimum in roughness observed for samples grown with bismuth BEPs in the range of 8×10^{-9}– 2.3×10^{-8} Torr, highlighted in blue in Fig. 1. The samples in this range exhibited smooth, droplet-free surface morphologies with RMS roughness measurements on the order of a reference InSb buffer layer (≤1.5 nm), which is suggestive of unity-sticking bismuth incorporation.

For samples grown with bismuth BEPs less than 8×10^{-9} Torr or greater than 2.3×10^{-8} Torr, droplet and/or nanostructure formation was present in AFM measurements, indicating non-substitutional bismuth incorporation. Similar observations were noted in the growth of $GaAs_{1-x}Bi_x$ as a function of the growth rate. Ptak *et al.* attributed droplet formation in samples with high bismuth content to ineffective incorporation of high bismuth fluxes while roughness in samples with low bismuth content was theorized to be due to an insufficient bismuth surfactant effect.[25] Another possible explanation for roughness in our films grown under low bismuth fluxes could be the formation of III-rich droplets/nanostructures due to growth with a total V flux less than necessary for stoichiometric growth. For $GaAs_{1-x}Bi_x$, Ptak *et al.* found that by increasing or decreasing the growth rate, the unity-sticking bismuth regime could be extended to include higher or lower bismuth concentrations, respectively.[25] While it is expected that the same behavior would hold true for $InSb_{1-x}Bi_x$, no systematic studies of the effects of growth rate on bismuth incorporation in $InSb_{1-x}Bi_x$ exist in the literature.

To quantify substitutional bismuth concentration in the $InSb_{1-x}Bi_x$ films with significant quantities of bismuth, high-resolution X-ray diffraction (HR-XRD) measurements were performed on six of the films with bismuth BEPs ≥ 8×10^{-9} Torr. HR-XRD coupled ω-2θ scans of the $InSb_{1-x}Bi_x$ films about the (004) peak of InSb exhibited increasingly compressively strained

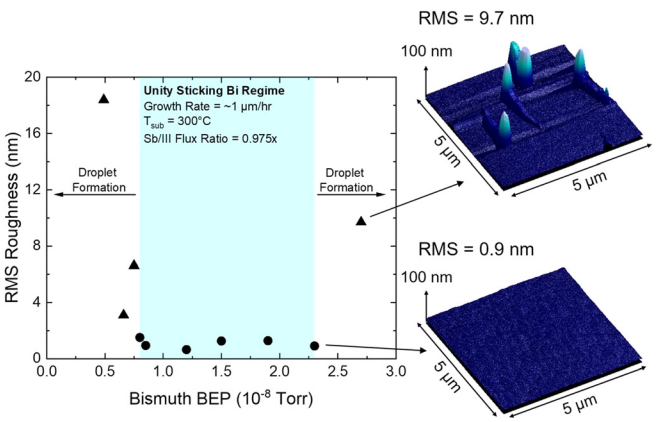

FIG. 1. AFM surface morphology measurements over a $5 \times 5\ \mu m^2$ area showed smooth surfaces (~1.5 nm RMS roughness or less) for films grown within an intermediate range of bismuth BEPs from 8×10^{-9} to 2.3×10^{-8} Torr. Outside of this range, the formation of droplets and nanostructures was evident. Surface morphology measurements of the two samples grown with the second highest bismuth BEP (bottom right) and highest bismuth BEP (top right) illustrate these two regimes respectively. This highlights a wide droplet-free growth window, which is a prerequisite for unity-sticking bismuth incorporation in $InSb_{1-x}Bi_x$.

layer peaks with increasing bismuth BEP, as shown in Fig. 2(a). Compressive strain is expected as several experimental investigations of $InAs_{1-x}Bi_x$,[17,26,27] $InSb_{1-x}Bi_x$,[12,28] and $InP_{1-x}Bi_x$[29,30] report zinc-blende InBi's lattice constant, estimated with extrapolation, as ranging from 6.5 to 7.3 Å, which is larger than that of InSb (6.48 Å). Dynamical simulations fit to the experimental XRD measurements suggested substitutional bismuth concentrations ranging from 0.45% to 1.9% in the films. Measured data and simulations for two of the samples are shown in Fig. 2(b). In these simulations, we assumed an InBi lattice constant of 6.626 Å based on extrapolations from Rutherford backscattering spectrometry (RBS) measurements of $InSb_{1-x}Bi_x$[12] and a Poisson's ratio of 0.3503 based on estimations from the well-established elastic coefficients of InP, InAs, and InSb.[26] Additionally, to best fit the measured data, a very thin (1.1–1.2 Å) interfacial layer was included at the interface between the substrate and the InSb buffer to account for any thin layer of In-based oxide that may have remained on the surface after thermal deoxidation.[31]

Importantly, the bismuth concentration in the films increased linearly with the bismuth BEP as seen in Fig. 2(c). This trend suggests unity-sticking incorporation; however, it is also necessary to quantify any non-substitutional incorporation of bismuth in the films. Historically, non-substitutional incorporation has plagued the dilute-borides,[32,33] dilute-nitrides,[34,35] and dilute-bismides[23,36,37] in the forms of antisite, interstitial, phase separated, and/or surface-segregated droplet formation.

To verify the mechanism(s) of incorporation, RBS measurements were performed on the same six $InSb_{1-x}Bi_x$ films to quantify the total bismuth content in the films. As seen in Fig. 3, the total bismuth concentration in the films increased linearly with increasing bismuth BEP for all samples, except for the film with the highest bismuth content, which possessed a rough surface morphology with droplet formation. It is worth noting that the differences in bismuth concentration extracted from XRD and RBS measurements could be due to small inaccuracies in the experimentally extrapolated zinc-blende InBi lattice constant.

The monotonic increase in both the substitutional and total bismuth concentration with increasing bismuth BEP in the samples with droplet-free surface morphologies, as measured by XRD and RBS respectively, strongly suggests that these films exhibit unity-sticking bismuth incorporation. As expected, there is also a clear linear relationship between the bismuth concentration as determined by RBS

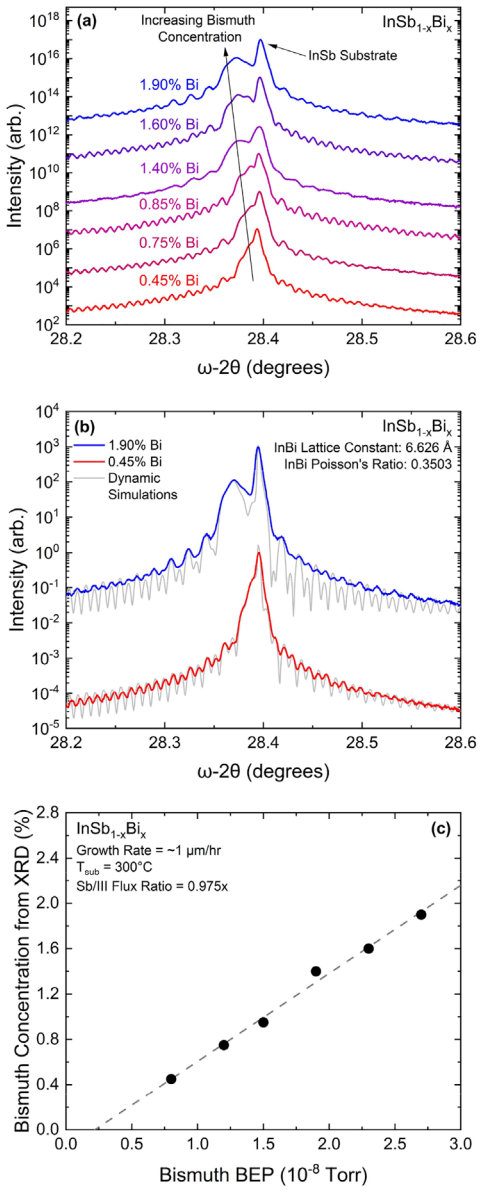

FIG. 2. (a) Coupled XRD ω-2θ scans of the six $InSb_{1-x}Bi_x$ films about the (004) peak of InSb. As expected, the compressively strained $InSb_{1-x}Bi_x$ layer peaks shifted to smaller angles with increasing bismuth flux. (b) Dynamical simulations of the films fit to the XRD measurements allowed estimation of the bismuth concentration in each sample assuming a zinc-blende InBi lattice constant of 6.626 Å. Representative simulations fit to the samples with the highest and lowest bismuth concentrations are shown. (c) Substitutional bismuth concentration increased linearly as a function of increasing bismuth BEP consistent with growth in the unity-sticking regime.

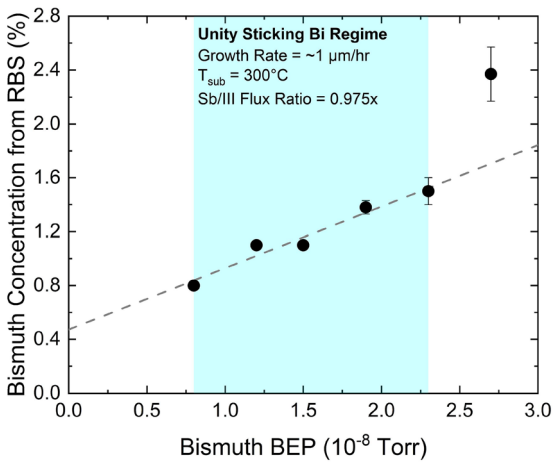

FIG. 3. Total bismuth concentration measured by RBS demonstrated a linear relationship between bismuth incorporation and bismuth BEP for a wide range of samples suggesting a unity-sticking regime that spans 0.8% to 1.5% bismuth incorporation under these growth conditions.

measurements and the strained lattice mismatch between the $InSb_{1-x}Bi_x$ layer peak and the substrate from XRD measurements for the samples grown within the unity-sticking bismuth regime. Furthermore, RBS channeling measurements performed on the sample containing the second highest concentration of bismuth indicated the bismuth was 98% substitutionally incorporated on the anion sublattice, approaching the sensitivity limit of the instrument. This strongly suggests that these five films were indeed grown under a kinetically limited growth regime and enables the identification of a range of bismuth concentrations from 0.8% to 1.5% (highlighted in blue in Figs. 1 and 3) that exhibit unity-sticking bismuth incorporation for the specific growth conditions employed in this report. In the remainder of this work, bismuth concentration values will be discussed based on XRD estimations, which represent the substitutional bismuth incorporation, except when otherwise noted.

From these films, PL from $InSb_{1-x}Bi_x$ was observed, likely owing to the optimized growth regime and, thus, high optical quality. Figure 4(a) shows the PL spectra of the films measured at 83 K. The peak at 5.45 μm was attributed to the InSb substrate, while the $InSb_{1-x}Bi_x$ film peaks exhibited wavelength extension as far as 6.5 μm at 83 K for the sample with the highest bismuth content. It should be noted that excitonic effects were assumed to be negligible as the exciton binding energy generally decreases with decreasing bandgap energy allowing for the assumption that the $InSb_{1-x}Bi_x$ exciton binding energy is <0.5 meV.[38] Correlating the bandgap reduction to the bismuth concentration in each sample by linear interpolation revealed a bismuth-induced bandgap reduction of $\sim$20 meV/% Bi based on XRD measurements of bismuth concentration, as seen in Fig. 4(b), or $\sim$29 meV/% Bi based on RBS measurements of bismuth concentration, as seen in Fig. 4(c). Since RBS channeling measurements showed extremely high substitutional bismuth incorporation, $\sim$29 meV/% Bi is likely the more accurate estimation of the effects of bismuth incorporation on the bandgap energy of $InSb_{1-x}Bi_x$. Bulk films tend to exhibit a peak PL energy approximately $0.5k_BT$ above the bandgap energy;[39,40] since the bismuth-induced bandgap reduction estimates are based on PL measurements all performed at the same temperature (83 K), there is no difference in trend between the peak PL energy and the bandgap energy as functions of bismuth concentration. Though there is nonlinearity in the bandgap reduction of $InSb_{1-x}Bi_x$ at very low bismuth concentrations ($<$0.8% based on RBS measurements), there is a strong linear relationship within the entirety of the identified unity-sticking bismuth regime. Additionally, $\sim$29 meV/% Bi is close to recent work from Rajpalke *et al.*, where a bismuth-induced bandgap reduction of 35 meV/% Bi based on optical absorption measurements of $InSb_{1-x}Bi_x$ at room temperature was demonstrated.[12] The full-width at half maximum (FWHM) as a function of bismuth concentration is also shown in Fig. 4(b). Within the unity-sticking bismuth regime, the FWHM increased from $\sim$10 meV for InSb to $\sim$25 meV with increasing bismuth concentration, likely due to alloy broadening.[41] However, the sample with the highest bismuth concentration exhibited a much higher FWHM of $\sim$95 meV, most likely due to inhomogeneous bismuth incorporation as a result of growth outside of the unity-sticking bismuth regime.

It is worth noting that for a typical highly mismatched alloy, PL intensity is expected to dramatically decrease with increasing concentration of the highly mismatched constituent as has been seen for various dilute-bismides.[13,14] However, in the $InSb_{1-x}Bi_x$ films, PL intensity was generally greater in the samples with higher bismuth incorporation. This suggests that PL strength is not dominated by

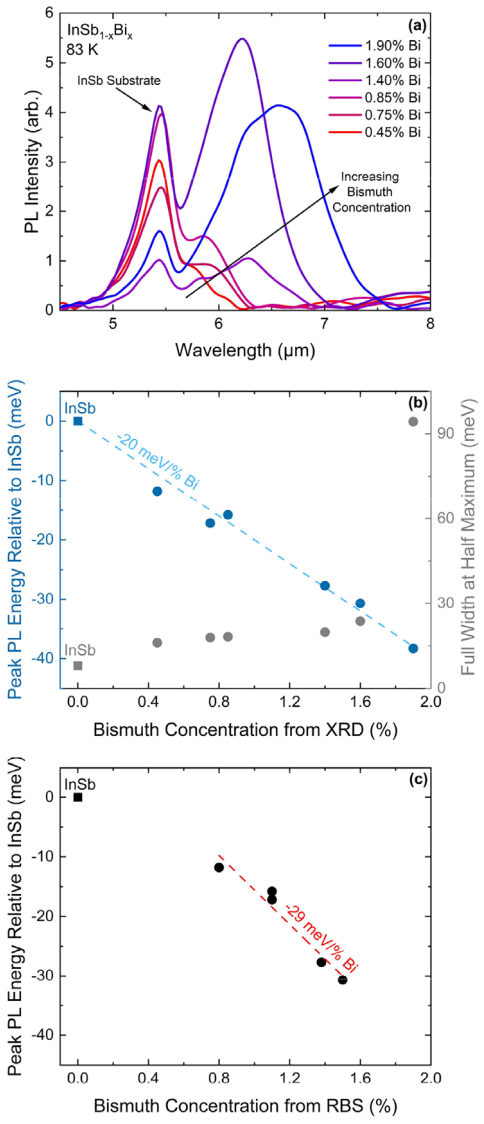

FIG. 4. (a) PL spectra measured at 83 K of $InSb_{1-x}Bi_x$ films with varying bismuth concentration demonstrating wavelength extension to 6.5 μm for the sample with the greatest bismuth concentration (1.9% Bi based on XRD measurements). (b) Peak PL energy (left, blue) as a function of bismuth concentration demonstrated a bismuth-induced bandgap reduction of $\sim$20 meV/% Bi based on XRD measurements. FWHM (right, gray) increased slightly with increasing bismuth concentration within the unity-sticking bismuth regime, likely due to alloy broadening. Outside of this regime, the sample with the highest bismuth concentration exhibited a much greater FWHM. (c) Within the unity-sticking bismuth regime, peak PL energy decreased by $\sim$29 meV/% Bi based on RBS measurements of total bismuth concentration.

bismuth concentration in $InSb_{1-x}Bi_x$ grown under these growth conditions, which could be very promising for $InSb_{1-x}Bi_x$-based optoelectronic devices operating at extended wavelengths.

To characterize the temperature-dependence of the bandgap, PL measurements were performed on the sample with the highest bismuth content (1.9% Bi based on XRD measurements) at temperatures ranging from 83 to 230 K, shown in Fig. 5(a). The peak PL energy

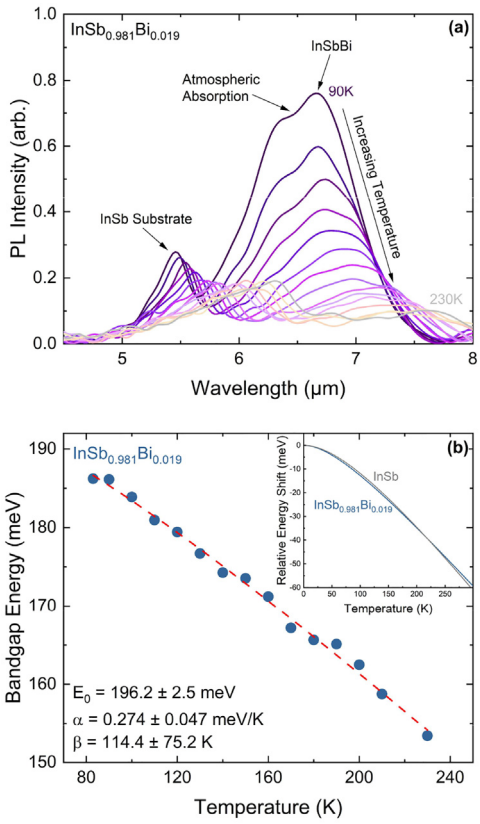

FIG. 5. (a) PL spectra of the $InSb_{1-x}Bi_x$ film containing the highest bismuth concentration at temperatures ranging from 83 to 230 K demonstrated a shift to longer wavelengths with increasing temperature as expected for an interband optical transition in a traditional III–V alloy. Note that the feature at ~6.5 μm is due to atmospheric H_2O absorption. (b) A Varshni fit to the bandgap energy as a function of temperature yielded α and β parameters comparable to traditional III–V alloys. Inset: A normalized Varshni fit of $InSb_{0.981}Bi_{0.019}$ compared favorably with the temperature dependence of the bandgap of bulk InSb.

decreased with increasing temperature, which is consistent with interband transitions in conventional III–V semiconductors. As seen in Fig. 5(b), a Varshni fit to the bulk bandgap energy, estimated as $0.5k_BT$ below the peak PL energy,[39,40] yielded reasonable α and β parameters, 0.274 meV/K and 114.4 K respectively, which compare favorably to those of typical III–V binaries. It should be noted that without colder measurements below 83 K, E_0 and β are relatively unconstrained [see error bars noted in Fig. 5(b)] and that lower temperature measurements would be necessary to fully confirm the temperature dependence of $InSb_{0.981}Bi_{0.019}$. While large degrees of bismuth inhomogeneity would manifest as broadening of the $InSb_{1-x}Bi_x$ layer peak in XRD measurements as seen in other dilute-bismide alloys,[26,42] there could be small degrees of bismuth clustering and/or localization that would only be observed in low temperature photoluminescence measurements in the form of an S-shape deviation from typical Varshni behavior[43] and/or a broad Urbach tail below the bandgap energy.[44] At the elevated temperatures measured in this work, Varshni fits of both $InSb_{0.981}Bi_{0.019}$ and InSb[45] demonstrated remarkably similar behavior as a function of temperature for the dilute-bismide alloy and the conventional III–V binary, shown in the inset of Fig. 5(b).

In conclusion, high-quality $InSb_{1-x}Bi_x$ films were grown by MBE. Unity-sticking bismuth incorporation was achieved as evidenced by smooth surface morphologies paired with linear trends in substitutional and total bismuth concentration as a function of bismuth flux. This was further supported by RBS channeling measurements, which showed a high proportion of substitutionally incorporated bismuth. Consequently, we observed PL from $InSb_{1-x}Bi_x$ and demonstrated wavelength extension out to 7.6 μm at 230 K. From these PL measurements, we estimated a bismuth-induced bandgap reduction of ~29 meV/% Bi at 83 K. Furthermore, temperature-dependent PL exhibited behavior consistent with what is observed from direct interband transitions in typical III–V alloys. The optimized growth window identified in this work, as well as the high-quality alloys grown in this regime, suggest that $InSb_{1-x}Bi_x$ is a particularly promising candidate for accessing the LWIR with high-quality III–V epitaxial devices.

See the supplementary material for the raw RBS measurements of the $InSb_{1-x}Bi_x$ films used to determine the total bismuth concentrations in each sample.

This work was performed in part at the University of Texas Microelectronics Research Center, a member of the National Nanotechnology Coordinated Infrastructure (NNCI), which was supported by the NSF (No. ECCS-1542159). This work was also supported by Lockheed Martin, the NSF (Award Nos. ECCS-1933836 and ECCS-1926187), and an NSF Graduate Fellowship (RCW).

The authors would like to acknowledge the Laboratory for Surface Modification at Rutgers University for conducting the RBS measurements and EAG Laboratories for conducting the RBS ion channeling measurement.

AUTHOR DECLARATIONS

Conflict of Interest

The authors have no conflicts to disclose.

Author Contributions

Rachel Corey White: Conceptualization (lead); Data curation (lead); Formal analysis (lead); Investigation (lead); Writing – original draft (lead). **Leland Nordin:** Data curation (supporting); Investigation (supporting); Writing – review & editing (equal). **Aaron Joseph Muhowski:** Data curation (supporting); Investigation (supporting); Writing – review & editing (equal). **Daniel Wasserman:** Funding acquisition (equal); Resources (equal); Supervision (equal); Writing – review & editing (supporting). **Seth R. Bank:** Funding acquisition (equal); Resources (equal); Supervision (equal); Writing – review & editing (supporting).

DATA AVAILABILITY

The data that support the findings of this study are available from the corresponding author upon reasonable request.

REFERENCES

[1]S. Francoeur, M. J. Seong, A. Mascarenhas, S. Tixier, M. Adamcyk, and T. Tiedje, Appl. Phys. Lett. **82**, 3874 (2003).

[2]M. P. Polak, P. Scharoch, and R. Kudrawiec, Semicond. Sci. Technol. **30**, 094001 (2015).
[3]R. Richards, F. Bastiman, C. J. Hunter, A. R. Mohmad, J. P. R. David, and N. Ekins-Daukes, in Proceedings of the IEEE 39th Photovoltaic Specialists Conference (2013).
[4]P. Ludewig, N. Knaub, N. Hossain, S. Reinhard, L. Nattermann, I. P. Marko, S. R. Jin, K. Hild, S. Chatterjee, W. Stolz, S. J. Sweeney, and K. Volz, Appl. Phys. Lett. **102**, 242115 (2013).
[5]Y. Gu, Y. G. Zhang, X. Y. Chen, Y. J. Ma, S. P. Xi, B. Du, and H. Li, Appl. Phys. Lett. **108**, 032102 (2016).
[6]S. Tixier, M. Adamcyk, T. Tiedje, S. Francoeur, A. Mascarenhas, P. Wei, and F. Schiettekatte, Appl. Phys. Lett. **82**, 2245 (2003).
[7]G. V. Rodriguez and J. M. Millunchick, J. Appl. Phys. **120**, 125310 (2016).
[8]W. A. Harrison, *Electronic Structure and the Properties of Solids: The Physics of the Chemical Bond* (W. H. Freeman and Company, San Francisco, 1980).
[9]E. Michel, G. Singh, S. Slivken, C. Besikci, P. Bove, I. Ferguson, and M. Razeghi, Appl. Phys. Lett. **65**, 3338 (1994).
[10]A. L. Allred, J. Inorg. Nucl. Chem. **17**, 215–221 (1961).
[11]A. Jean-Louis, B. Ayrault, and J. Vargas, Phys. Status Solidi B **34**, 341 (1969).
[12]M. K. Rajpalke, W. M. Linhart, K. M. Yu, M. Birkett, J. Alaria, J. J. Bomphrey, S. Sallis, L. F. J. Piper, T. S. Jones, M. J. Ashwin, and T. D. Veal, Appl. Phys. Lett. **105**, 212101 (2014).
[13]M. Masnadi-Shirazi, R. B. Lewis, V. Bahrami-Yekta, T. Tiedje, M. Chicoine, and P. Servati, J. Appl. Phys. **116**, 223506 (2014).
[14]O. Delorme, L. Cerutti, E. Tournié, and J. B. Rodriguez, J. Cryst. Growth **477**, 144–148 (2017).
[15]J. Devenson, V. Pačebutas, R. Butkuté, A. Baranov, and A. Krotkus, Appl. Phys. Express **5**, 015503 (2012).
[16]S. T. Schaefer, R. R. Kosireddy, P. T. Webster, and S. R. Johnson, J. Appl. Phys. **126**, 083101 (2019).
[17]S. J. Maddox, H. P. Nair, V. D. Dasika, E. M. Krivoy, R. Salas, and S. R. Bank, in Proceedings of the 54th Electronic Materials Conference (2012).
[18]A. Rogalski, P. Martyniuk, and M. Kopytko, Appl. Phys. Rev. **4**, 031304 (2017).
[19]B. F. Levine, J. Appl. Phys. **74**, R1 (1993).
[20]J. J. Lee, J. D. Kim, and M. Razeghi, Appl. Phys. Lett. **70**, 3266 (1997).
[21]Y. Song, S. Wang, I. S. Roy, P. Shi, A. Hallen, and Z. Lai, J. Cryst. Growth **378**, 323–328 (2013).
[22]K. Oe, S. Ando, and K. Sugiyama, Jpn. J. Appl. Phys. **20**, L303 (1981).
[23]S. C. Das, T. D. Das, and S. Dhar, Infrared Phys. Technol. **55**, 306–308 (2012).
[24]S. G. Spruytte, C. W. Coldren, A. F. Marshall, M. C. Larson, and J. S. Harris, MRS Internet J. Nitride Semicond. Res. **5**, 474–480 (2000).
[25]A. J. Ptak, R. France, D. A. Beaton, K. Alberi, J. Simon, A. Mascarenhas, and C. S. Jiang, J. Cryst. Growth **338**, 107–110 (2012).
[26]A. J. Shalindar, P. T. Webster, B. J. Wilkens, T. L. Alford, and S. R. Johnson, J. Appl. Phys. **120**, 145704 (2016).
[27]K. Oe and H. Okamoto, Jpn. J. Appl. Phys. **37**, L1283–L1285 (1998).
[28]B. Joukoff and A. M. Jean-Louis, J. Cryst. Growth **12**, 169–172 (1972).
[29]Y. Gu, K. Wang, H. Zhou, Y. Li, C. Cao, L. Zhang, Y. Zhang, Q. Gong, and S. Wang, Nanoscale Res. Lett. **9**, 24 (2014).
[30]K. Wang, Y. Gu, H. F. Zhou, L. Y. Zhang, C. Z. Kang, M. J. Wu, W. W. Pan, P. F. Lu, Q. Gong, and S. M. Wang, Sci. Rep. **4**, 5449 (2014).
[31]W. K. Liu and M. B. Santos, J. Vac. Sci. Technol. B **14**, 647 (1996).
[32]V. K. Gupta, M. W. Koch, N. J. Watkins, Y. Gao, and G. W. Wicks, J. Electron. Mater. **29**, 12 (2000).
[33]M. E. Groenert, R. Averbeck, W. Hosler, M. Schuster, and H. Riechert, J. Cryst. Growth **264**, 123–127 (2004).
[34]S. G. Spruytte, C. W. Coldren, W. Wampler, P. Krispin, K. Ploog, M. C. Larson, and J. S. Harris, J. Appl. Phys. **89**, 8 (2001).
[35]M. Reason, H. A. McKay, W. Ye, S. Hanson, V. Rotberg, and R. S. Goldman, Appl. Phys. Lett. **85**, 1692 (2004).
[36]H. Fitouri, I. Moussa, A. Rebey, A. Fouzri, and B. El Jani, J. Cryst. Growth **295**, 114–118 (2006).
[37]A. J. Noreika, W. J. Takei, M. H. Francombe, and C. E. C. Wood, J. Appl. Phys. **53**, 7 (1982).
[38]J. K. Kübler, Phys. Status Solidi **35**, 189 (1969).
[39]Z. M. Fang, K. T. Ma, D. J. Jaw, R. M. Cohen, and G. B. Stringfellow, J. Appl. Phys. **67**, 7034 (1990).
[40]B. E. A. Saleh and M. C. Teich, *Fundamentals of Photonics* (John Wiley & Sons, Hoboken, NJ, 2007).
[41]E. F. Schubert, E. O. Göbel, Y. Horikoshi, K. Ploog, and H. J. Queisser, Phys. Rev. B **30**, 813 (1984).
[42]A. R. Mohmad, F. Bastiman, C. J. Hunter, R. D. Richards, S. J. Sweeney, J. S. Ng, J. P. R. David, and B. Y. Majlis, Phys. Status Solidi B **251**, 1276–1281 (2014).
[43]S. Mazzucato, H. Lehec, H. Carrere, H. Makhloufi, A. Arnoult, C. Fontaine, T. Amand, and X. Marie, Nanoscale Res. Lett. **9**, 19 (2014).
[44]C. Gogineni, N. A. Riordan, S. R. Johnson, X. Lu, and T. Tiedje, Appl. Phys. Lett. **103**, 041110 (2013).
[45]I. Vurgaftman, J. R. Meyer, and L. R. Ram-Mohan, J. Appl. Phys. **89**, 5815 (2001).